



**HAL**  
open science

## High-spin states above the isomers in neutron-rich iodine nuclei near $N = 82$

R. Banik, S. Bhattacharyya, M. Rejmund, A. Lemasson, S. Biswas, A. Navin, Y. Kim, C. Michelagnoli, I. Stefan, P. Bednarczyk, et al.

► **To cite this version:**

R. Banik, S. Bhattacharyya, M. Rejmund, A. Lemasson, S. Biswas, et al.. High-spin states above the isomers in neutron-rich iodine nuclei near  $N = 82$ . *Physical Review C*, 2020, 102 (4), pp.044329. 10.1103/PhysRevC.102.044329 . hal-02986928

**HAL Id: hal-02986928**

**<https://hal.science/hal-02986928>**

Submitted on 14 Nov 2020

**HAL** is a multi-disciplinary open access archive for the deposit and dissemination of scientific research documents, whether they are published or not. The documents may come from teaching and research institutions in France or abroad, or from public or private research centers.

L'archive ouverte pluridisciplinaire **HAL**, est destinée au dépôt et à la diffusion de documents scientifiques de niveau recherche, publiés ou non, émanant des établissements d'enseignement et de recherche français ou étrangers, des laboratoires publics ou privés.

# High spin states above the isomers in neutron rich Iodine nuclei near $N = 82$

R. Banik,<sup>1,2,\*</sup> S. Bhattacharyya,<sup>1,2,†</sup> M. Rejmund,<sup>3</sup> A. Lemasson,<sup>3</sup> S. Biswas,<sup>3</sup> A. Navin,<sup>3</sup> Y.H. Kim,<sup>3,‡</sup> C. Michelagnoli,<sup>3,‡</sup> I. Stefan,<sup>4</sup> P. Bednarczyk,<sup>5</sup> Soumik Bhattacharya,<sup>1,2</sup> E. Clément,<sup>3</sup> H.L. Crawford,<sup>6</sup> G. de France,<sup>3</sup> P. Fallon,<sup>6</sup> G. Frémont,<sup>3</sup> J. Goupil,<sup>3</sup> B. Jacquot,<sup>3</sup> H.J. Li,<sup>3</sup> J. Ljungvall,<sup>7</sup> A. Maj,<sup>5</sup> L. Ménager,<sup>3</sup> V. Morel,<sup>3</sup> G. Mukherjee,<sup>1,2</sup> R. Palit,<sup>8</sup> R.M. Pérez-Vidal,<sup>9</sup> J. Ropert,<sup>3</sup> and C. Schmitt<sup>3</sup>

<sup>1</sup>Variable Energy Cyclotron Centre, 1/AF Bidhannagar, Kolkata 700064, India

<sup>2</sup>Homi Bhabha National Institute, Training School Complex, Anushaktinagar, Mumbai-400094, India

<sup>3</sup>GANIL, CEA/DRF-CNRS/IN2P3, Bd Henri Becquerel, BP 55027, F-14076 Caen Cedex 5, France

<sup>4</sup>Institut de Physique Nucleaire, IN2P3-CNRS, Univ. Paris Sud,  
Universite Paris Saclay, 91406 Orsay Cedex, France

<sup>5</sup>Institute of Nuclear Physics PAN, 31-342 Kraków, Poland

<sup>6</sup>Nuclear Science Division, Lawrence Berkeley National Laboratory, Berkeley, California 94720, USA

<sup>7</sup>CSNSM, Univ. Paris-Sud, CNRS/IN2P3, Université Paris-Saclay, 91405 Orsay, France

<sup>8</sup>Department of Nuclear and Atomic Physics, Tata Institute of Fundamental Research, Mumbai, 400005, India

<sup>9</sup>Instituto de Física Corpuscular, CSIC-Universitat de València, E-46980 València, Spain

(Dated: October 5, 2020)

Excited states of neutron rich Iodine isotopes  $^{130-134}\text{I}$  above the high spin isomers have been identified using prompt-delayed  $\gamma$ -ray spectroscopy. The Iodine isotopes have been produced as fission fragments of fusion-fission and transfer induced fission of  $^9\text{Be}(^{238}\text{U}, f)$  at a beam energy of 6.2 MeV/u. The complete  $(A, Z)$  identification was obtained using the large acceptance magnetic spectrometer VAMOS++. The AGATA  $\gamma$ -ray tracking array was used to detect the prompt  $\gamma$  rays while the delayed  $\gamma$  rays (in the time range of 100 ns to 200  $\mu\text{s}$ ) from the isomeric states were identified by the EXOGAM segmented Clover detectors, placed behind the focal plane of VAMOS++ spectrometer. The high spin states above the  $(8^-)$  isomers in  $^{130,132}\text{I}$  have been populated for the first time and a new isomer in  $^{132}\text{I}$  has been identified. New  $\gamma$ -ray transition has also been assigned to the level structure of  $^{134}\text{I}$ . Prompt transitions above the  $19/2^-$  isomer have been identified in  $^{131,133}\text{I}$ , for the first time. The level structures are interpreted in terms of the systematics of odd- $Z$  nuclei above  $Z = 50$  shell closure and large scale shell model calculations.

## I. INTRODUCTION

The nuclei with either odd numbers of valence protons (odd- $Z$ ) or odd numbers of valence neutrons (odd- $N$ ) near a major shell closure were always of special interests as their level structures carry an important link to nucleon-nucleon effective interaction [1–3]. The doubly magic  $^{132}\text{Sn}$  ( $Z = 50, N = 82$ ) has a robust shell closure having its first excited state at 4.0 MeV [4]. Thus, the single particle excitations, particle-hole interactions and mixing of various single particle configurations in nuclei with few valence particles/holes around  $^{132}\text{Sn}$  have been the subject of contemporary interest, both experimentally [5–9] and theoretically [2, 10]. In particular, nuclei with a few odd valence protons outside  $Z = 50$  shell with few neutron holes in  $N = 82$  shell, provide important information about the multiplets of various particle-hole configurations. The excited states of these nuclei also provide key inputs in understanding the effective interactions used for large scale shell model calculations. The presence of high- $j$ , unique parity  $h_{11/2}$  orbital

in  $Z, N = 50 - 82$  shell, for both protons and neutrons, plays the major role in generating the high spin states for nuclei in  $A = 130$  region. Configurations involving  $h_{11/2}$  neutron holes are also responsible for systematic occurrence of isomers in odd- $A$  as well as in odd-odd nuclei in this region. It would be thus interesting to investigate the level structure above these isomers to understand the involvement of  $h_{11/2}$  orbital and relative contribution of proton and neutron occupancies in this high- $j$  orbital in generating the high spin states above the isomers.

The Iodine ( $Z = 53$ ) isotopes with three protons outside  $Z = 50$  and a few neutron holes/particles in vicinity of the  $N = 82$  have attracted attention of several recent studies. The importance of several structures based on  $\pi g_{7/2}$ ,  $\pi d_{5/2}$  and  $\nu h_{11/2}$  orbitals has been reported systematically in odd-odd Iodine isotopes till  $N = 75$  [11–14]. In odd- $A$  Iodine isotopes  $^{127,129}\text{I}$ , collective bands based on  $\pi g_{7/2}$ ,  $\pi d_{5/2}$  and  $\pi h_{11/2}$  configurations have been reported. At higher spins, the states associated with a neutron pair breaking, involving orbitals  $\pi g_{7/2}$  and  $\nu h_{11/2}$ , have also been observed [15, 16]. Towards the  $N = 82$ , isomeric states ( $19/2^-$  and  $23/2^+$ ) dominated by two neutron-hole configurations coupled to the odd number of protons have been identified in  $^{131,133}\text{I}$  ( $N = 78, 80$ ) [17].

The spectroscopic information on high spin states above the isomers of neutron-rich Iodine isotopes in  $A \sim 130$  mass region, towards  $N = 82$ , is very lim-

\*Present address: Institute of Engineering and Management, Saltlake Sector V, Kolkata 700091, India.

†Corresponding author; Electronic address: [sarmi@vecc.gov.in](mailto:sarmi@vecc.gov.in)

‡Present address: Institut Laue-Langevin, F-38042 Grenoble Cedex, France.

ited. This is mainly because of the fact that these nuclei are at the limit of accessibility using fusion evaporation reactions, which could be used to produce the isotopes till  $^{129}\text{I}$ . For heavier isotopes, either multi-nucleon transfer reactions [17] or spontaneous fission of  $^{252}\text{Cf}$  [18] or  $^{248}\text{Cm}$  [19–21] are used to study the high spin excitations. Studies of the spontaneous fission of actinides utilize the prompt high-fold  $\gamma$ - $\gamma$  coincidence technique to identify the high spin states. With this technique, it is not possible to obtain  $\gamma$ - $\gamma$  correlations across long lived isomers. In these studies, neutron-rich Iodine nuclei, above  $N = 82$  shell closure, could be studied [20–23]. In contrast, for neutron-rich Iodine isotopes  $^{130,132}\text{I}$ , just below  $N = 82$ , almost no information on high spin states is available. Low lying long lived high spin isomers,  $(6^-)$ ,  $(8^-)$ , have been identified systematically in odd-odd neutron-rich Iodine isotopes. Few states above the  $(8^-)$  isomer ( $T_{1/2} = 3.52$  min) in  $^{134}\text{I}$  [18], have been identified, but no excited states above the corresponding  $(8^-)$  isomers in  $^{132}\text{I}$  ( $T_{1/2} = 1.38$  hr) and in  $^{130}\text{I}$  ( $T_{1/2} = 315$  ns) were reported.

In the present work, the neutron-rich Iodine isotopes  $^{130-134}\text{I}$  were produced as fission fragments and their excited states have been characterized from in-beam prompt-delayed  $\gamma$ -ray spectroscopy after isotopic identification ( $A, Z$ ). The high spin excitations above the  $(8^-)$  isomer and the corresponding  $\gamma$ -ray transitions in odd-odd Iodine nuclei  $^{130,132}\text{I}$  have been observed for the first time. A new isomer in  $^{132}\text{I}$  has been identified and the half-life has been measured from the corresponding  $\gamma$ -ray decay. New prompt  $\gamma$ -ray transitions above the isomeric states in  $^{131,133}\text{I}$  and  $^{134}\text{I}$  have also been identified. Using large scale shell model calculations, the contribution of the neutron hole occupancy of the  $\nu h_{11/2}$  orbital to the high spin negative parity states is analyzed.

## II. EXPERIMENT AND DATA ANALYSIS

The excited states of neutron rich Iodine isotopes were populated via fusion-fission and transfer induced fission reactions in inverse kinematics, using a  $^{238}\text{U}$  beam of energy 6.2 MeV/u bombarding a  $^9\text{Be}$  target of thickness 1.6  $\mu\text{m}$  and 5  $\mu\text{m}$  at Grand Accélérateur National d'Ions Lourds (GANIL). The isotopic identification ( $A, Z$ ) of the fission fragments was obtained using the large acceptance magnetic spectrometer VAMOS++, placed at an angle of  $20^\circ$  with respect to the beam axis [24–28]. The  $Z$  identification was obtained by  $\Delta E$ - $E$  measurement using the ionization chamber placed at the focal plane of VAMOS++. Time of Flight of each fragment was measured using a Dual Position-Sensitive Multi-Wire Proportional Counter (DPS-MWPC) [27] placed at the entrance of VAMOS++ and the MWPC placed at the focal plane. The focal plane detector system also consisted of two drift chambers (DC) for tracking. The mass number ( $A$ ), atomic number ( $Z$ ), atomic charge ( $Q$ ) and the velocity vector of the fission fragments were determined

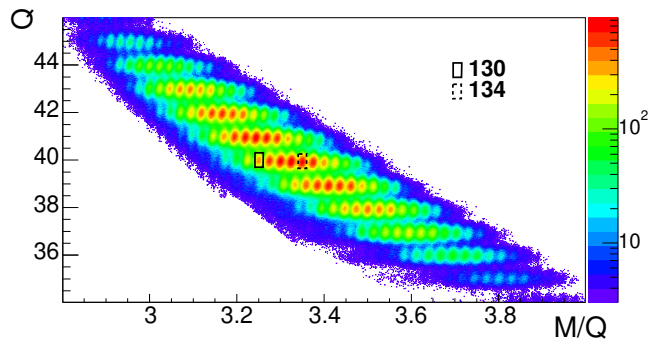


FIG. 1: Charge state ( $Q$ ) as a function of the mass over charge ( $M/Q$ ) after the selection of Iodine ( $Z = 53$ ). The Iodine isotopes are obtained from various charge states and the identification of  $A = 130$  and  $134$  are marked for charge state  $Q = 40$ .

on an event-by-event basis. The  $(M/Q)$  parameter was obtained from the reconstructed magnetic rigidity ( $B\rho$ ) and velocity of the fragment. The resolution (FWHM) achieved for  $Z$ ,  $A$  and  $Q$  are 1.3%, 0.4% and 1.3% respectively. The nuclei were identified individually following their  $Z$  ( $\Delta E - E$ ),  $A$  and  $Q$  ( $Q - M/Q$ ) selection. The narrow gates were applied to obtain the corresponding  $\gamma$ -ray spectra. The identification of Iodine isotopes obtained from the two-dimensional plot of  $Q$  and  $M/Q$  is shown in Fig. 1. Further details and identification spectra are given in Ref. [28]. The possible contamination of the  $\gamma$ -ray spectra by the nuclei associated with the neighboring  $Z$ ,  $A$  and  $Q$  were individually examined. The analysis of the corresponding  $\gamma$ -ray spectra allowed to evaluate any possible small contamination and perform the suitable background subtraction case-by-case.

The prompt  $\gamma$  rays ( $\gamma_P$ ) emitted from the recoiling fission products at the target position were detected using position sensitive  $\gamma$ -ray tracking array AGATA [29]. In the current experimental setup, AGATA consisted of 32 crystals and was placed at 13.5 cm away from the target. As the nuclei fly away from the target, the AGATA array does not detect  $\gamma$  rays emitted after few ns. No lifetime information was extracted using the  $\gamma$  rays detected in AGATA. The data was acquired under the condition of a coincidence between the prompt  $\gamma$  rays and DPS-MWPC within 300 ns. The typical time of flight for the Iodine isopes in VAMOS++ was  $\sim 200$  ns. An array of seven EXOGAM segmented Clover detectors [30] was also placed behind the ionization chamber of VAMOS++ in a wall configuration to detect the delayed  $\gamma$  rays ( $\gamma_D$ ). The trigger for detecting the delayed  $\gamma$  rays detected at EXOGAM detectors was generated when a delayed  $\gamma$ -ray followed the prompt trigger within 200  $\mu\text{s}$ . The time between the ion implantation and the delayed  $\gamma$ -ray event was measured using time stamp differences obtained using 100 MHz clock. The time resolution of EXOGAM detectors was  $\sim 6$  ns at 1 MeV. The decay curves were obtained from the time difference between

the signals from the DPS-MWPC placed at the entrance of VAMOS++ and the EXOGAM detectors placed at the focal plane, and thus the time measured is independent of the time of flight. Due to the use of logic delays in the trigger the time ( $t_{Decay}$ ) has 800 ns offset, thus the true reaction time corresponds to a  $t_{Decay} = 800$  ns. The shortest lifetimes measured in the focal plane using the present experimental setup is  $T_{1/2} = 60(20)$  ns and  $90(16)$  ns in  $^{126}\text{Sb}$  [31]. Further details of the experimental setup consisting VAMOS++, AGATA and EXOGAM can be found in Ref. [28].

Coincidence matrices were constructed between prompt  $\gamma$  rays ( $\gamma_P$ - $\gamma_P$ ), prompt-delayed  $\gamma$  rays ( $\gamma_P$ - $\gamma_D$ ) and any two delayed  $\gamma$  rays ( $\gamma_D$ - $\gamma_D$ ) [28]. Also, small corrections for isobaric and isotopic contamination (if any) were taken into account for each of the Iodine isotopes in both prompt and delayed spectra following the procedure described in Ref. [28]. Intensity determination and corrections for half-lives calculations have also been carried out, as described in Ref. [28]. The spin-parities of the excited states were tentatively assigned based on systematics of Iodine isotopes and shell-model calculations.

### III. RESULTS

#### A. $^{130}\text{I}$

Prior to the present study, the spectroscopic information of  $^{130}\text{I}$  was investigated via  $(n, \gamma)$ ,  $(d, p)$  reactions using two Ge(Li) detectors [32] and also via  $(^3\text{He}, t)$  reaction [33]. Half-lives of four isomeric states at 39.95 keV ( $8.3 \pm 1.0$  min), 69.58 keV ( $133 \pm 7$  ns), 82.39 keV ( $315 \pm 15$  ns) and 85.10 keV ( $254 \pm 4$  ns) were also reported in Ref. [32] with probable spin-parity assignments as  $(2^+)$ ,  $(6^-)$ ,  $(8^-)$  and  $(6^-)$  respectively. The 82.39 keV level was assigned as  $(8^-)$  in Ref. [32], though, this assignment for the 82.39 keV level was not adopted in Ref. [34]. No high spin states above the  $(6^-)$  or  $(8^-)$  isomers have been reported for  $^{130}\text{I}$  prior to the present work.

Prompt-delayed spectroscopy of isotopically identified fission fragment gives the unique opportunity to investigate the high spin excited states of this isotope above the isomers. Fig. 2 shows the proposed level scheme of  $^{130}\text{I}$ , obtained from the present work. All the transitions placed in the level scheme above the isomeric state were observed for the first time and are marked in red. The relative placements of these  $\gamma$ -ray transitions in the level scheme were done based on their mutual coincidence relationships and relative intensities. The details of the  $\gamma$  rays of  $^{130}\text{I}$  with tentative spin and parity of the initial ( $J_i^\pi$ ) and the final ( $J_f^\pi$ ) states are given in Table I. Fig. 3(a) shows the prompt singles  $\gamma$ -ray spectrum ( $\gamma_P$ ) after Doppler correction, in coincidence with the  $^{130}\text{I}$  fragments. A coincidence spectrum corresponding to the sum of gates on 748, 922 and 971 keV transitions is shown in Fig. 3(b). The 748, 922, 135 and 971 keV  $\gamma$

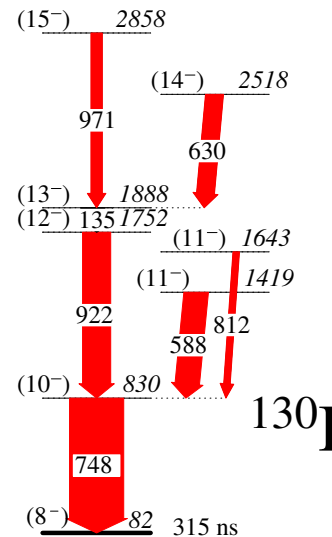


FIG. 2: Level scheme of  $^{130}\text{I}$  above the  $(8^-)$  isomeric level, as obtained in the present work. The newly observed  $\gamma$  rays are displayed in red. The thickness of the  $\gamma$  rays represents their relative intensities.

rays were found to be in mutual coincidence, whereas, the 588 and 812 keV  $\gamma$  rays were observed only in coincidence with the 748 keV  $\gamma$ -ray. This is evident from the coincidence spectra corresponding to the 588 and 922 keV transitions shown in Fig. 3(c) and Fig. 3(d) respectively. Similarly, the 630 keV  $\gamma$ -ray was found to be in coincidence with the 748-922-135 keV cascade, but not with the 971, 588 and 812 keV  $\gamma$  rays. A coincidence spectrum corresponding to the 630 keV  $\gamma$ -ray gate is also shown in Fig. 3(e), where the presence of the 748, 922 and 135 keV  $\gamma$  rays is clearly visible. Other transitions, *i.e.*, 397, 465, 607 keV  $\gamma$  rays are also observed in prompt spectrum and are marked in Fig. 3(a), but no coincidence could be obtained with other prompt  $\gamma$  rays in  $^{130}\text{I}$ , observed in the present work. These transitions were also previously reported in Ref. [32], but the  $\gamma$  rays which are reported to be in coincidence with these transitions in Ref. [32], are not observed in the present work. There are a few more  $\gamma$  rays of energies 340, 375, 444, 557, 738 and 1091 keV, which are identified as belonging to  $^{130}\text{I}$  and marked in the total singles spectrum (Fig. 3(a)), but could not be placed in the level scheme due to lack of coincidence information.

The isomers in  $^{130}\text{I}$  decay via low energy  $\gamma$ -ray transitions ( $E_\gamma < 100$  keV). The low energy cutoff for the delayed  $\gamma$ -ray spectra in the present setup was around 80-100 keV, thus the decay  $\gamma$  rays from these low lying isomers could not be observed in the delayed spectrum obtained in the present work. Therefore, the definite placement of the observed sequence of prompt transitions above the particular isomeric state is not possible. However, following the systematics of neighboring even-*A* Iodine isotopes, the observed prompt  $\gamma$  rays from the present work have been placed above the  $(8^-)$  isomer.



TABLE II: Energies ( $E_\gamma$ ) and relative intensities ( $I_\gamma$ ) of the  $\gamma$  rays observed in  $^{131}\text{I}$  along with spin and parity of the initial ( $J_i^\pi$ ) and the final ( $J_f^\pi$ ) states and the energy of the initial state ( $E_i$ ). The top and bottom panels, separated by a line, are for the prompt and delayed transitions, respectively. The intensity scales of prompt and delayed transitions are different. The low energy transitions which could not be detected with the present setup are adopted from Ref.[17] and are put within bracket.

$E_\gamma(\text{Err})$ (keV)	$E_i$ (keV)	$I_\gamma(\text{Err})$	$J_i^\pi \rightarrow J_f^\pi$
201.1(1)	3039.8	10(1)	$(27/2^+) \rightarrow (25/2^+)$
240.7(3)	1795.5	6(2)	$15/2^- \rightarrow 15/2^+$
325.2(2)	1879.9	23(9)	$15/2^+ \rightarrow 15/2^+$
330.9(2)	1885.6	6(2)	$17/2^- \rightarrow 15/2^+$
348.6(2)	4243.7	11(3)	$(29/2^-) \rightarrow (27/2^-)$
352.2(2)	2232.2	10(1)	$19/2^+ \rightarrow 15/2^+$
358.2(3)	2590.4	14(2)	$(21/2^+) \rightarrow 19/2^+$
490.5(1)	2838.7	35(1)	$(25/2^+) \rightarrow 23/2^+$
563.6(1)	3603.4	27(2)	$(29/2^+) \rightarrow (27/2^+)$
677.5(1)	2232.2	30(3)	$19/2^+ \rightarrow 15/2^+$
691.8(1)	3039.8	46(2)	$(27/2^+) \rightarrow 23/2^+$
773.1(1)	773.1	100	$11/2^+ \rightarrow 7/2^+$
781.6(2)	1554.7	59(2)	$15/2^+ \rightarrow 11/2^+$
822.3(1)	1595.4	12(2)	$13/2^+ \rightarrow 11/2^+$
851.9(1)	851.9	28(2)	$9/2^+ \rightarrow 7/2^+$
949.1(1)	2866.7	34(1)	$(23/2^-) \rightarrow 19/2^-$
1028.4(1)	3895.1	15(2)	$(27/2^-) \rightarrow (23/2^-)$
1106.9(3)	1879.9	8(1)	$15/2^+ \rightarrow 11/2^+$
(32)	1917.6	-	$19/2^- \rightarrow 17/2^-$
(116)	2348.2	-	$23/2^+ \rightarrow 19/2^+$
122.1(1)	1917.6	34(5)	$19/2^- \rightarrow 15/2^-$
199.9(2)	1795.5	14(4)	$15/2^- \rightarrow 13/2^+$
743.8(1)	1595.6	15(2)	$13/2^+ \rightarrow 9/2^+$

prompt singles  $\gamma$ -ray ( $\gamma_P$ ) spectrum (Fig. 5(a)), but are not present in prompt coincidence with 773 or 782 keV (Fig. 5(b)). Prompt  $\gamma$  rays in coincidence with added gates of 692, 491, 201 and 564 keV  $\gamma$  rays, confirming the transitions placed above the  $23/2^+$  (42 ns) isomeric level, are shown in Fig. 5(c). The other prompt  $\gamma$  rays above  $23/2^+$  level, reported in Ref. [17], of energy 765, 1055, 1202, 702, 1266 keV, could not be observed in the present work. Fig. 5(d) represents the coincidence gate of 1028 keV transition, which shows that the 949 and 349 keV  $\gamma$  rays are in prompt coincidence with 1028 keV. But these  $\gamma$  rays are not in prompt coincidence with any other transitions placed in  $^{131}\text{I}$ .

Fig. 6(a) shows the delayed singles  $\gamma$ -ray ( $\gamma_D$ ) spectrum obtained with EXOGAM detectors for  $t_{\text{Decay}} < 75 \mu\text{s}$ , following the procedure described in Ref. [28]. All the delayed  $\gamma$  rays below the 1918 keV ( $19/2^-$ ) isomeric level are seen in this spectrum. The decay curve corresponding to the 122 + 331 keV delayed  $\gamma$  rays is shown in the inset of Fig. 6(a) within the same time window. An exponential fit to the time decay corresponding to the added gates of 122 and 331 keV  $\gamma$  rays yield a half-life of  $T_{1/2} = 24.6(52) \mu\text{s}$  for the 1918 keV ( $19/2^-$ ) level from the present measurements. The measured half-life of the 1918 keV ( $19/2^-$ ) level corroborates the reported value of 24(1)  $\mu\text{s}$  [17]. The delayed  $\gamma$ -ray ( $\gamma_D$ ) spectrum for

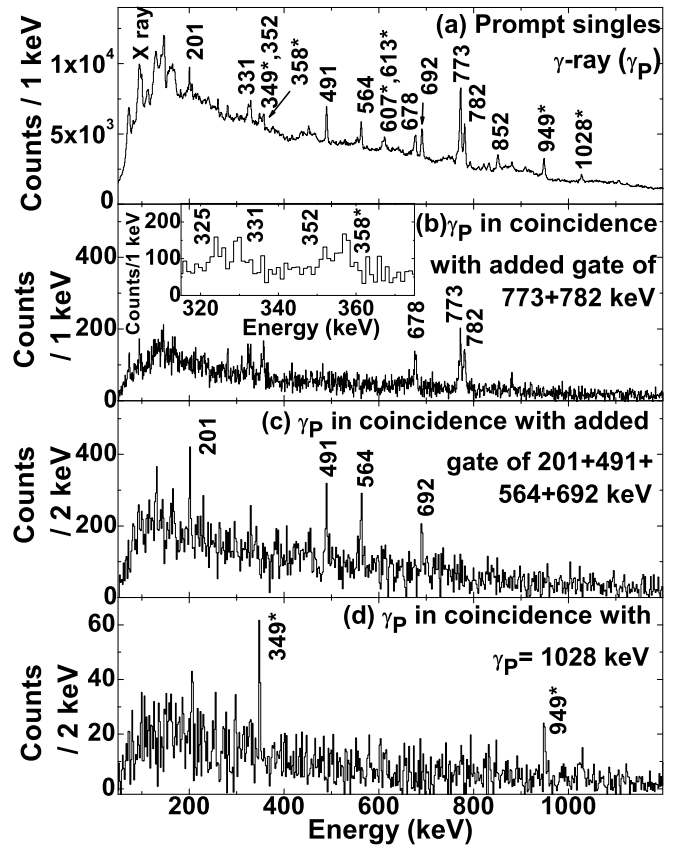


FIG. 5: (a) The prompt singles  $\gamma$ -ray spectrum of  $^{131}\text{I}$ . (b) Prompt  $\gamma$  rays ( $\gamma_P$ ) in coincidence with added gates of  $\gamma_P = 773 + 782$  keV. The inset shows the expanded energy range of 300-400 keV. (c) Prompt  $\gamma$  rays ( $\gamma_P$ ) in coincidence with added gates of  $\gamma_P = 201 + 491 + 564 + 692$  keV. (d) Prompt  $\gamma$  rays ( $\gamma_P$ ) in coincidence with  $\gamma_P = 1028$  keV. The new  $\gamma$ -transitions are marked with ‘\*’.

$t_{\text{Decay}} < 75 \mu\text{s}$  in coincidence with the newly observed prompt transition of 949 keV is shown in Fig. 6(b). The delayed  $\gamma$  rays de-exciting the  $19/2^-$  isomeric level are seen in this spectrum. This confirms the placement of the 949 keV prompt  $\gamma$ -ray above the 1918 keV ( $19/2^-$ ) isomeric level. Fig. 6(c) shows the prompt  $\gamma$ -ray ( $\gamma_P$ ) spectrum corresponding to the gate on the delayed  $\gamma$ -ray 122 keV. The presence of the 949 keV  $\gamma$ -ray in this coincidence spectrum and the mutual prompt coincidence among the 949, 1028 and 349 keV  $\gamma$  rays (as shown in Fig. 5(d)) establishes the placement of prompt  $\gamma$ -ray cascade of 949-1028-349 keV above the 1918 keV ( $19/2^-$ ) isomeric level. The  $\gamma$  rays of this sequence are placed according to their intensities.

### C. $^{132}\text{I}$

Excited states of  $^{132}\text{I}$  were studied earlier using  $\beta$ -decay of  $^{132}\text{Te}$ , produced from the  $\alpha$ -induced fission [39]. In this  $\beta$ -decay study, only the low spin states were popu-

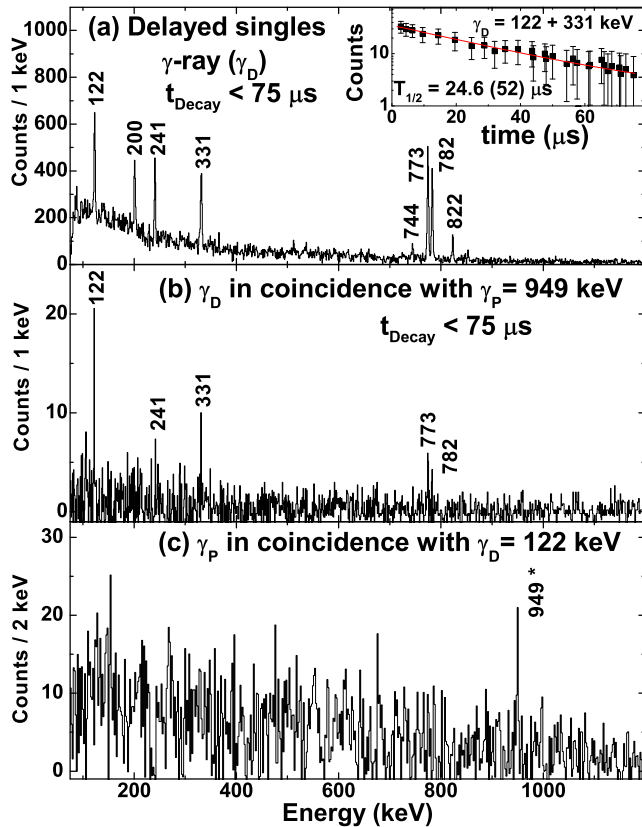


FIG. 6: (a) The delayed singles  $\gamma$ -ray ( $\gamma_D$ ) spectrum of  $^{131}\text{I}$  for  $t_{Decay} < 75 \mu\text{s}$ . The inset shows the decay curve of  $\gamma_D = 122 + 331$  keV delayed transitions with exponential fit. (b) Delayed  $\gamma$  rays ( $\gamma_D$ ) for  $t_{Decay} < 75 \mu\text{s}$  in coincidence with  $\gamma_P = 949$  keV. (c) Prompt  $\gamma$  rays ( $\gamma_P$ ) in coincidence with  $\gamma_D = 122$  keV. The new  $\gamma$ -transitions are marked with ‘\*’.

lated. The lifetime and magnetic moment measurements of low spin states have been reported in various investigations [40–42]. The presence of an isomeric state ( $8^-$ ,  $T_{1/2} = 83.6 \pm 1.7$  min) at 120 keV excitation was also reported in Ref. [39, 41], it was populated in  $\alpha$ -induced fission reaction. No information of the high spin states above this long lived ( $8^-$ ) isomer was available.

The proposed level scheme of  $^{132}\text{I}$ , as obtained from the present work, is shown in Fig. 7. All the  $\gamma$  rays, marked in the level scheme with red color, are observed for the first time. The  $\gamma$  rays are placed in the level scheme according to their prompt-prompt and prompt-delayed coincidence relations and relative intensities. The proposed level scheme (Fig. 7) from the present work is placed on top of the ( $8^-$ ) isomeric state. No coincidences were observed between the previously known transitions and the newly observed  $\gamma$  rays from the present work. Due to the very long lifetime of the ( $8^-$ ) isomer, prompt-delayed coincidence measurement across this isomer was not possible in the present experiment. The details of the  $\gamma$  rays of  $^{132}\text{I}$  with tentative spin and parity of the initial ( $J_i^\pi$ ) and the final ( $J_f^\pi$ ) states are tabulated in Table III. A

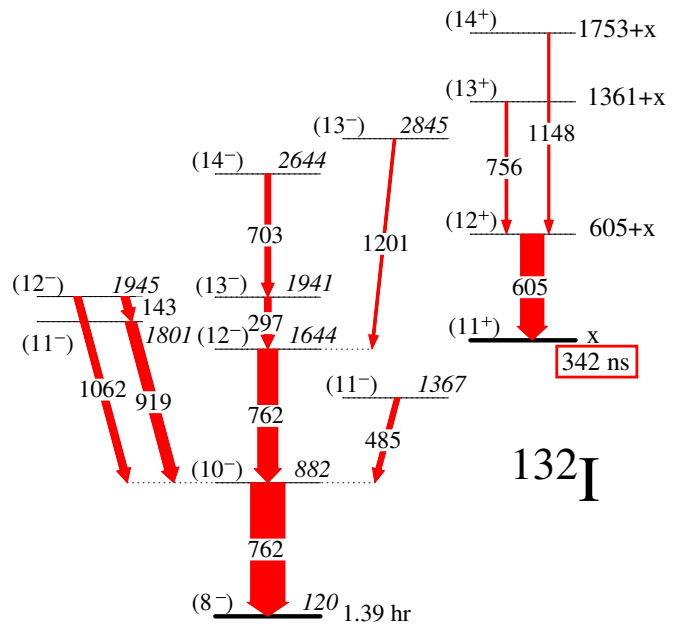


FIG. 7: Level scheme of  $^{132}\text{I}$  above the ( $8^-$ ) isomeric level, as obtained in the present work. The newly observed  $\gamma$  rays are displayed in red. Isomeric state is indicated with a thick line and the newly measured half-life has been marked with a red box. The thickness of the  $\gamma$  rays represents their relative intensities with respect to the 762 keV doublet.

TABLE III: Energies ( $E_\gamma$ ) and relative intensities ( $I_\gamma$ ) of the  $\gamma$  rays observed in  $^{132}\text{I}$  along with probable spin and parity of the initial ( $J_i^\pi$ ) and the final ( $J_f^\pi$ ) states and the energy of the initial state ( $E_i$ ). The total intensity of the 762 keV doublet is normalized to 100.

$E_\gamma$ (Err) (keV)	$E_i$ (keV)	$I_\gamma$ (Err)	$J_i^\pi \rightarrow J_f^\pi$
143.3(2)	1944.6	12(2)	( $12^-$ ) $\rightarrow$ ( $11^-$ )
296.9(1)	1941.3	12(1)	( $13^-$ ) $\rightarrow$ ( $12^-$ )
484.6(1)	1366.8	10(1)	( $11^-$ ) $\rightarrow$ ( $10^-$ )
605.4(1)	605+x	44(1)	( $12^+$ ) $\rightarrow$ ( $11^+$ )
703.0(1)	2644.3	11(2)	( $14^-$ ) $\rightarrow$ ( $13^-$ )
755.7(2)	1361+x	2(1)	( $13^+$ ) $\rightarrow$ ( $12^+$ )
762.2(4)	1644.4	100 <sup>d</sup>	( $12^-$ ) $\rightarrow$ ( $10^-$ )
762.2(4)	882.2		( $10^-$ ) $\rightarrow$ ( $8^-$ )
919.2(3)	1801.4	21(2)	( $11^-$ ) $\rightarrow$ ( $10^-$ )
1062.4(2)	1944.6	14(1)	( $12^-$ ) $\rightarrow$ ( $10^-$ )
1147.8(2)	1753+x	4(1)	( $14^+$ ) $\rightarrow$ ( $12^+$ )
1200.9(2)	2845.3	5(2)	( $13^-$ ) $\rightarrow$ ( $12^-$ )

Doppler corrected prompt singles  $\gamma$ -ray ( $\gamma_P$ ) spectrum, obtained with AGATA, in coincidence with  $^{132}\text{I}$  fragments, isotopically ( $A, Z$ ) identified at the focal plane of the VAMOS++ spectrometer, is shown in Fig. 8(a). In this spectrum, the new  $\gamma$  rays observed from the present work are marked with ‘\*’. A prompt  $\gamma$ - $\gamma$  coincidence spectrum corresponding to the gate of 762 keV  $\gamma$ -ray is shown in Fig. 8(b). Presence of a 762 keV transition in the 762 keV gate establishes 762 keV as a doublet transition. Other than the 762 keV, the 143, 297, 485, 703, 919, 1062 and 1201 keV transitions are also found to be in

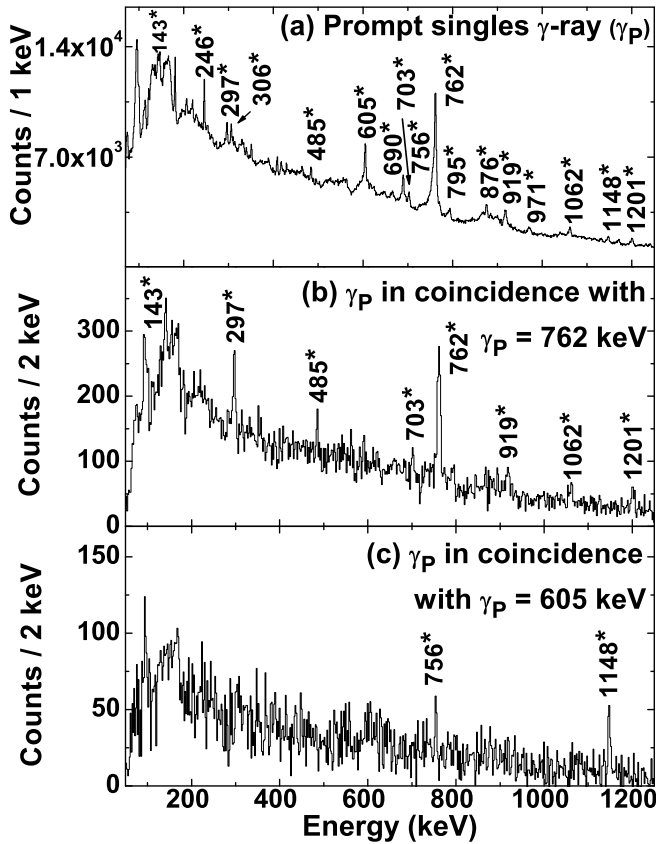


FIG. 8: (a) The prompt singles  $\gamma$ -ray spectrum of  $^{132}\text{I}$ . (b) Prompt  $\gamma$  rays ( $\gamma_P$ ) in coincidence with  $\gamma_P = 762$  keV. (c) Prompt  $\gamma$  rays ( $\gamma_P$ ) in coincidence with  $\gamma_P = 605$  keV. The new  $\gamma$ -transitions are marked with ‘\*’.

coincidence with the 762 keV  $\gamma$ -ray. The 762 keV doublet and the other transitions observed in the 762 keV gate are placed in the level scheme of  $^{132}\text{I}$  (Fig. 7) according to their relative intensities. Among the transitions observed in the 762 keV gate, the 297, 485, 919, 1062 and 1201 keV are not found to be in coincidence with each other. The 143 keV transition is found to be in coincidence with 762 keV and 919 keV transitions, but not with the 1062 keV. Thus, the 919-143 keV cascade is placed in parallel with the 1062 keV from coincidence relationship, intensities and energy sum. The observed intensity of the 762 keV in the coincidence spectra of the 297, 919, 1062 and 1201 keV gates is compared to understand the relative placements of these transitions in the level scheme. The intensity of the 762 keV is found to be more in the coincidence spectra of the 297 and 1201 keV gates than that in the coincidence spectra of the 1062 and 919 keV gates, after appropriate intensity normalization of the gating transitions. Thus, it is clear that the 1062 and 919 keV  $\gamma$  rays are in coincidence with one of the transitions of the 762 keV doublet, whereas, 297 and 1201 keV are in coincidence with both the transitions of the 762 keV doublet. Also the 605, 756 and 1148 keV  $\gamma$  rays are seen in the

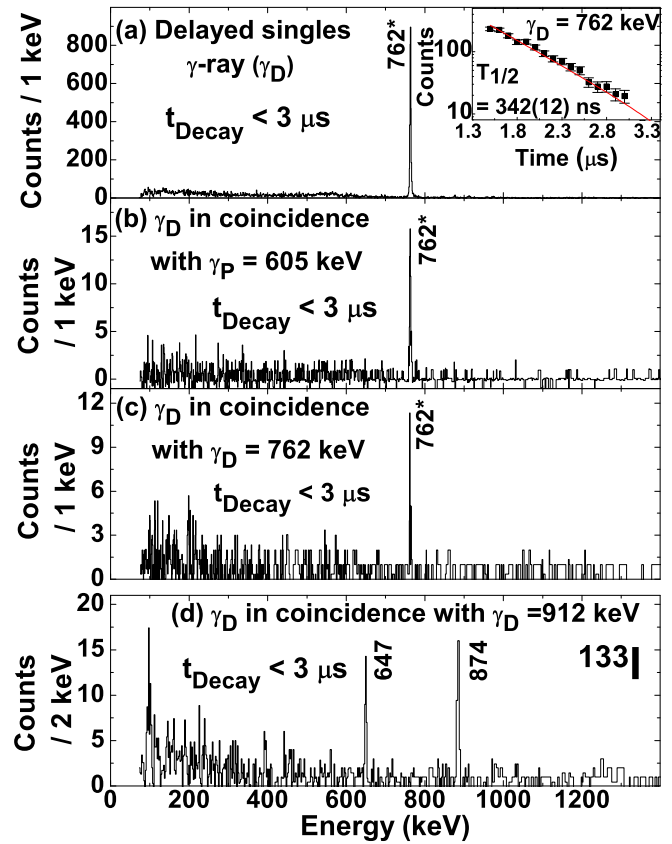


FIG. 9: (a) The delayed singles  $\gamma$ -ray ( $\gamma_D$ ) spectrum of  $^{132}\text{I}$  for  $t_{\text{Decay}} < 3 \mu\text{s}$ . The inset shows the decay pattern of delayed  $\gamma$ -ray 762 keV with exponential fitting. (b) Delayed  $\gamma$  rays ( $\gamma_D$ ) for  $t_{\text{Decay}} < 3 \mu\text{s}$  in coincidence with  $\gamma_P = 605$  keV. (c) Delayed  $\gamma$  rays ( $\gamma_D$ ) for  $t_{\text{Decay}} < 3 \mu\text{s}$  in coincidence with  $\gamma_D = 762$  keV. (d) Delayed  $\gamma$  rays ( $\gamma_D$ ) for  $t_{\text{Decay}} < 3 \mu\text{s}$  in coincidence with  $\gamma_D = 912$  keV of  $^{133}\text{I}$ . The new  $\gamma$ -transitions are marked with ‘\*’.

prompt singles ( $\gamma_P$ ) spectrum (Fig. 8(a)), but are not in coincidence with the 762 keV (Fig. 8(b)). The 756 and 1148 keV transitions are found to be present in the coincidence spectrum corresponding to the 605 keV gate as shown in Fig. 8(c). On the other hand, no coincidence could be found between the 756 and 1148 keV transitions and hence these are placed in parallel with each other. The set of transitions of energy 605, 756 and 1148 keV do not have any prompt coincidence with any other  $\gamma$  rays of the prompt sequence. The  $\gamma$  rays of energies 246, 306, 690, 795 and 876 keV, observed in the prompt singles  $\gamma$ -ray spectrum (Fig. 8(a)), could not be placed in the level scheme of  $^{132}\text{I}$ , as these are not observed to be in coincidence with other  $\gamma$  rays in  $^{132}\text{I}$ .

The delayed singles  $\gamma$ -ray ( $\gamma_D$ ) spectrum obtained with the EXOGAM detectors for  $t_{\text{Decay}} < 3 \mu\text{s}$  is shown in Fig. 9(a). Only 762 keV transition was found to be in this delayed coincidence. The inset of Fig. 9(a) shows the fitting of the decay curve of the 762 keV transition, from which the half-life is obtained as  $T_{1/2} = 342(12)$  ns.



TABLE IV: Energies ( $E_\gamma$ ) and relative intensities ( $I_\gamma$ ) of the  $\gamma$  rays observed in  $^{133}\text{I}$  along with probable spin and parity of the initial ( $J_i^\pi$ ) and the final ( $J_f^\pi$ ) states and the energy of the initial state ( $E_i$ ). The top and bottom panels, separated by a line, are for the prompt and delayed transitions, respectively. The low energy transitions which could not be detected with the present setup are adopted from Ref. [17] and are put within bracket.

$E_\gamma(\text{Err})$ (keV)	$E_i$ (keV)	$I_\gamma(\text{Err})$	$J_i^\pi \rightarrow J_f^\pi$
154.6(1)	4046.3	12(2)	$(27/2^+) \rightarrow (25/2^+)$
226.2(1)	4675.3	18(1)	$(31/2^+) \rightarrow (29/2^+)$
352.8(2)	2433.2	3(1)	$19/2^+ \rightarrow 15/2^+$
378.5(1)	1937.6	12(1)	$(17/2^-) \rightarrow 15/2^+$
436.2(2)	5111.5	10(1)	$(33/2^+) \rightarrow (31/2^+)$
521.3(1)	2080.5	3(1)	$15/2^+ \rightarrow 15/2^+$
535.6(2)	3854.2	25(3)	$(27/2^-) \rightarrow (25/2^-)$
614.0(1)	3105.9	54(1)	$(25/2^+) \rightarrow 23/2^+$
629.2(1)	4449.1	21(1)	$(29/2^+) \rightarrow (27/2^+)$
647.0(1)	1559.1	41(2)	$15/2^+ \rightarrow 11/2^+$
714.0(1)	3819.9	26(1)	$(27/2^+) \rightarrow (25/2^+)$
729.2(1)	3318.6	26(2)	$(25/2^-) \rightarrow (23/2^-)$
785.8(1)	3891.7	25(1)	$(25/2^+) \rightarrow (25/2^+)$
862.7(1)	1774.8	18(2)	$13/2^+ \rightarrow 11/2^+$
874.1(1)	2433.2	15(1)	$19/2^+ \rightarrow 15/2^+$
912.1(1)	912.1	100	$11/2^+ \rightarrow 7/2^+$
956.3(1)	2589.4	31(2)	$(23/2^-) \rightarrow 19/2^-$
1168.4(1)	2080.5	3(1)	$15/2^+ \rightarrow 11/2^+$
(59)	2491.9	-	$23/2^+ \rightarrow 19/2^+$
(74)	1633.1	-	$19/2^- \rightarrow 15/2^+$
(95)	1728.1	-	$15/2^- \rightarrow 19/2^-$
(169)	1728.1	-	$15/2^- \rightarrow 15/2^+$

It may be noted that, a similar set of prompt  $\gamma$  rays have been observed in the neighboring odd- $A$   $^{131}\text{I}$ , above the  $19/2^-$  isomer (24.6  $\mu\text{s}$ ). Thus, it is possible that the new cascade of prompt transitions of 956-729-536 keV, observed in  $^{133}\text{I}$  may also decay to the  $19/2^-$  (9 sec) isomeric state. As the upper limit (200  $\mu\text{s}$ ) of the delayed time window for the present setup is much lower than the half-life of the  $19/2^-$  (9 sec) isomeric state in  $^{133}\text{I}$ , the prompt-delayed correlation across the isomer cannot be obtained. Therefore, the cascade of prompt transitions of 956-729-536 keV is placed above the  $19/2^-$  (9 sec) isomeric state at 1633 keV in  $^{133}\text{I}$ .

Fig. 12(a) shows the delayed singles  $\gamma$ -ray ( $\gamma_D$ ) spectrum for  $t_{\text{Decay}} < 3 \mu\text{s}$ . All the known delayed  $\gamma$  rays of  $^{133}\text{I}$ , *i.e.*, 912, 647, 874, 1168 and 353 keV, are observed in this time gated delayed spectrum. The other known delayed low energy  $\gamma$  rays of 59, 74, 95, 169 keV could not be observed in this delayed spectrum, either due to their weak intensities or due to the low energy threshold of the present setup to detect delayed  $\gamma$  rays. The time decay curve for the 874 + 353 + 1168 keV transitions, decaying out from the  $23/2^+$  isomer is shown in the inset of Fig. 12(a). An exponential decay fit of this curve yields a value of  $T_{1/2} = 478(17)$  ns, which matches well with the reported [17] value of 469(15) ns. Fig. 12(b) shows the delayed  $\gamma$  rays observed in coincidence with the prompt transitions of 614, 714, 629 and 785 keV above the  $23/2^+$  isomer. The known delayed transitions of 912, 647 and

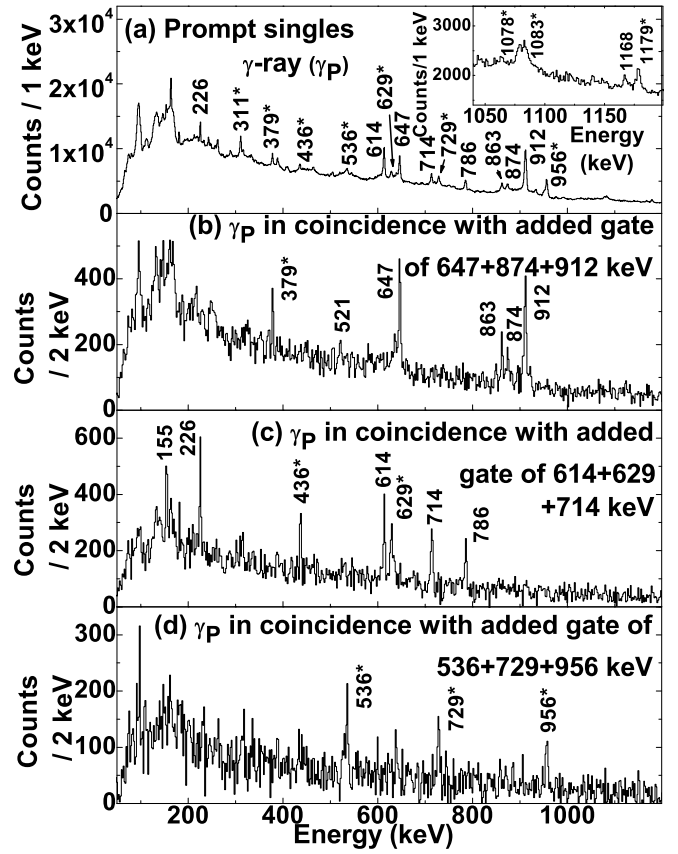


FIG. 11: (a) The prompt singles  $\gamma$ -ray spectrum of  $^{133}\text{I}$ . The higher energy part of this spectrum is shown in an expanded scale in the inset. (b) Prompt  $\gamma$  rays ( $\gamma_P$ ) in coincidence with the added gate of  $\gamma_P = 647 + 874 + 912$  keV. (c) Prompt  $\gamma$  rays ( $\gamma_P$ ) in coincidence with added gate of  $\gamma_P = 614 + 629 + 714$  keV. (d) Prompt  $\gamma$  rays ( $\gamma_P$ ) in coincidence with added gate of  $\gamma_P = 536 + 729 + 956$  keV. The new  $\gamma$ -transitions are marked with '\*' in all the cases.

874 keV below the isomer is clearly seen in this spectrum. The other  $\gamma$  rays of 353, 521 and 1168 keV could not be seen in this spectrum due to their weak intensities.

## E. $^{134}\text{I}$

Low lying excited states of  $^{134}\text{I}$  were previously studied from  $\beta$ -decay of  $^{134}\text{Te}$  [45, 46]. A high spin isomer ( $8^-$ ) of  $T_{1/2} \sim 3.8 \pm 0.2$  m (adopted in NNDC as  $3.52 \pm 0.04$  m [47]) at an excitation energy of 316 keV was also identified in Ref. [48]. High spin states above the ( $8^-$ ) isomer in  $^{134}\text{I}$  were recently investigated using prompt spectroscopy of fission fragments [18] where five excited states were identified. The assignment of  $\gamma$  rays to  $^{134}\text{I}$  was done in Ref. [18] on the basis of intensity distribution of its complementary fragments.

The level scheme of  $^{134}\text{I}$ , as obtained from the present measurements, is shown in Fig. 13. In the present work, the level scheme above the reported ( $8^-$ ) isomer of  $^{134}\text{I}$ ,

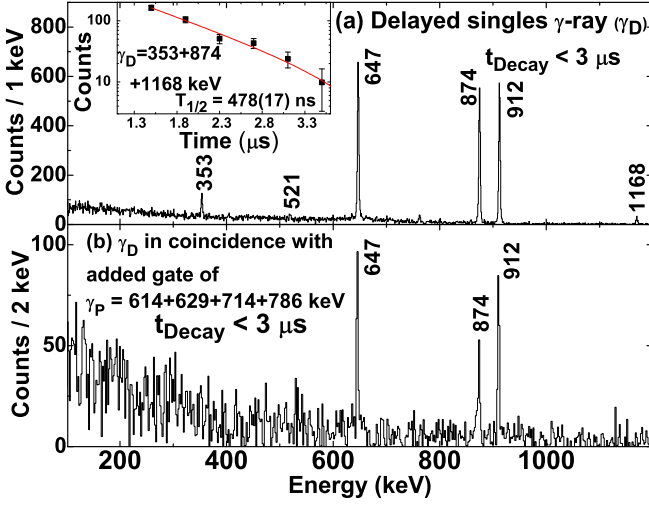


FIG. 12: (a) Delayed  $\gamma$ -ray ( $\gamma_D$ ) spectrum of  $^{133}\text{I}$  for  $t_{\text{Decay}} < 3 \mu\text{s}$ . Inset of the figure shows the decay pattern of delayed  $\gamma$  rays  $\gamma_D = 353 + 874 + 1168$  keV with exponential fitting. (b) Delayed  $\gamma$  rays ( $\gamma_D$ ) in coincidence with the added prompt gate of  $\gamma_P = 614 + 629 + 714 + 786$  keV.

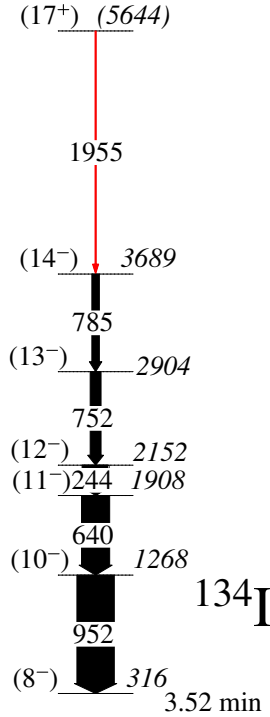


FIG. 13: Level scheme of  $^{134}\text{I}$  as obtained in the present work. The newly observed  $\gamma$  rays are displayed in red. The thickness of the  $\gamma$  rays represents their relative intensity.

as reported by Liu *et al.* [18], is extended with the placement of one new  $\gamma$ -ray transition  $(17^+) \rightarrow (14^-)$  above 3689 keV level (see discussions Section IV B). The assignment of the earlier known  $\gamma$  rays and the newly observed  $\gamma$ -ray from the present work is confirmed after unambiguous isotopic ( $A, Z$ ) identification of  $^{134}\text{I}$ . The details

TABLE V: Energies ( $E_\gamma$ ) and relative intensities ( $I_\gamma$ ) of the  $\gamma$  rays observed in  $^{134}\text{I}$  along with probable spin and parity of the initial ( $J_i^\pi$ ) and the final ( $J_f^\pi$ ) states and the energy of the initial state ( $E_i$ ).

$E_\gamma$ (Err) (keV)	$E_i$ (keV)	$I_\gamma$ (Err)	$J_i^\pi \rightarrow J_f^\pi$
243.5(1)	2150.9	68(1)	$(12^-) \rightarrow (11^-)$
639.6(1)	1907.4	75(1)	$(11^-) \rightarrow (10^-)$
752.0(1)	2902.9	29(2)	$(13^-) \rightarrow (12^-)$
785.2(1)	3688.1	20(1)	$(14^-) \rightarrow (13^-)$
951.8(1)	1267.8	100	$(10^-) \rightarrow (8^-)$
1955.1(1)	5643.2	3(1)	$(17^+) \rightarrow (14^-)$

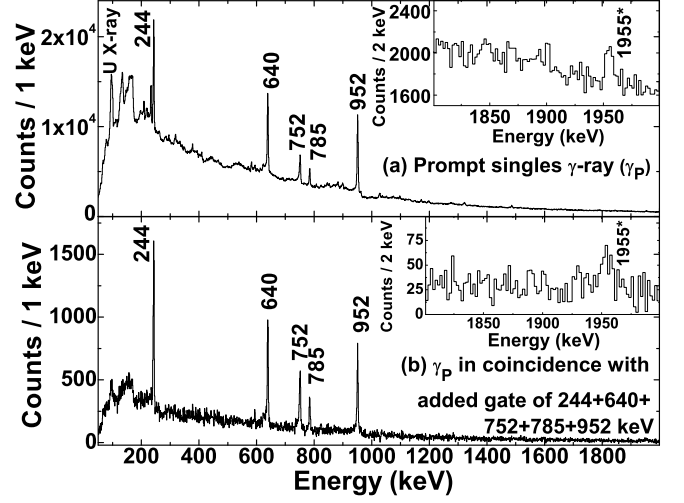


FIG. 14: (a) The prompt singles  $\gamma$ -ray spectrum of  $^{134}\text{I}$ . (b) Prompt  $\gamma$  rays ( $\gamma_P$ ) in coincidence with added gate of  $\gamma_P = 244 + 640 + 752 + 785 + 952$  keV. The higher energy part of the spectra are shown in insets. The new  $\gamma$ -transitions are marked with ‘\*’ in all the cases.

of the  $\gamma$  rays of  $^{134}\text{I}$  with probable spin and parity of the initial ( $J_i^\pi$ ) and the final ( $J_f^\pi$ ) states are tabulated in Table V. A Doppler corrected prompt singles  $\gamma$ -ray spectrum ( $\gamma_P$ ), obtained with AGATA, in coincidence with  $^{134}\text{I}$  fragments, is shown in Fig. 14(a). The previously known  $\gamma$ -ray transitions of energy 244, 640, 752, 785 and 952 keV are marked along with one new  $\gamma$ -ray of energy 1955 keV (marked with ‘\*’), observed from the present work. The prompt  $\gamma$ - $\gamma$  coincidence spectrum corresponding to the added prompt gates on 952, 640, 244, 752 and 785 keV transitions is shown in Fig. 14(b). All the previously assigned transitions along with 1955 keV (marked with ‘\*’) are seen in this figure. The presence of 1955 keV  $\gamma$ -ray in this added spectrum is clear from the inset of Fig. 14(b), where the higher energy part of the coincidence spectrum is shown in an expanded energy scale. The new transition is tentatively placed in the level scheme of  $^{134}\text{I}$ , based on the coincidence spectra shown in inset of Fig. 14(b), above the 3689 keV level. No delayed  $\gamma$  rays ( $\gamma_D$ ) could be observed in  $^{134}\text{I}$  in the present work.

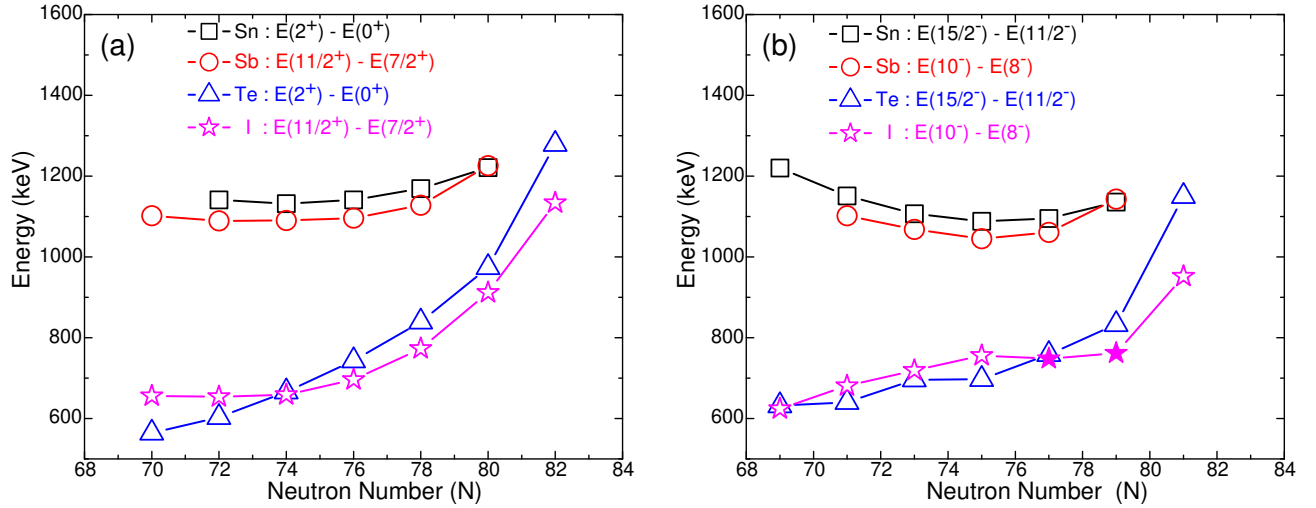


FIG. 15: Systematics of experimental energy differences for the lowest states with  $\Delta I = 2$  for: (a) even- $N$  isotopes of Sn ( $E(2^+) - E(0^+)$ ), Sb ( $E(11/2^+) - E(7/2^+)$ ), Te ( $E(2^+) - E(0^+)$ ) and I ( $E(11/2^+) - E(7/2^+)$ ). (b) odd- $N$  isotopes of Sn ( $E(15/2^-) - E(11/2^-)$ ), Sb ( $E(10^-) - E(8^-)$ ), Te ( $E(15/2^-) - E(11/2^-)$ ) and I ( $E(10^-) - E(8^-)$ ). The new states observed in the present measurements are shown by filled symbols.

## IV. DISCUSSION

### A. Systematics

The systematics of the energy difference between the lowest lying  $\Delta I = 2$  states is plotted for the isotopes of Sn ( $Z = 50$ ), Sb ( $Z = 51$ ), Te ( $Z = 52$ ) and I ( $Z = 53$ ) as a function of neutron number in Fig. 15(a) for even- $N$  and in Fig. 15(b) for odd- $N$ . One can observe the change in the energy differences as one, two and three protons are added to the corresponding Tin core ( $\text{Sn}_N$ ). In Sb, the energy differences  $E(11/2^+) - E(7/2^+)$  and  $E(10^-) - E(8^-)$  follow closely the corresponding  $E(2^+) - E(0^+)$  and  $E(15/2^-) - E(11/2^-)$  in Sn, respectively. This reflects the fact that the energy difference results from the neutron excitation, *i.e.*  $2^+$ , in both Sn and Sb, since the proton is either absent in Sn or singly present in Sb. It can be also seen that in I the energy differences  $E(11/2^+) - E(7/2^+)$  and  $E(10^-) - E(8^-)$  follow the corresponding  $E(2^+) - E(0^+)$  and  $E(15/2^-) - E(11/2^-)$  in Te, respectively. The significant drop in the energy difference in Te and I, relative to that in Sn and Sb, results from the strong mixing, between the proton and neutron excitations due to the neutron-proton interaction. The decrease of the energy differences in Te and I, towards the neutron mid-shell can be seen from the figure. The systematic energy drop, *i.e.*  $(Z, Z + 1), (Z + 2, Z + 3), \dots$  with  $Z = 50$ , is related to the increase of the collectivity. Similar energy drop and an energy inheritance, for odd- $Z$  from even- $Z$  isotones, could be also observed for other isotopes from the known data (not shown here) while more protons are added, towards the proton mid-shell.

### B. Shell Model Calculations

To understand the basic configurations and contribution of various single particle orbitals to the excited states of the Iodine isotopes in the mass region  $A = 130 - 134$ , observed in the present work, large scale shell model calculations have been performed using the code NUSHELLX [49]. The calculations were carried out using the model space involving  $1g_{7/2}, 2d_{5/2}, 2d_{3/2}, 3s_{1/2}, 1h_{11/2}$  single particle orbitals, for both protons and neutrons. The calculations used the SN100PN interaction [50]. The results of the shell model calculations are compared with the experimental levels, obtained in the present work, for even- $A$  and odd- $A$  Iodine isotopes in Fig. 16(a-c) and Fig. 16(d-e) respectively. An overall good agreement is observed between the experimental and calculated levels for all the Iodine isotopes.

In the present shell model calculation of the even mass isotopes  $^{130}\text{I}$  ( $N = 77$ ) and  $^{132}\text{I}$  ( $N = 79$ ), the  $8^-$  level is predicted as the ground state, instead for the experimentally known ground states of  $5^+$  and  $4^+$ , respectively. But, the energy difference between the calculated and experimental ground states are found to be within 120 keV for both the nuclei. In the case of  $^{134}\text{I}$  ( $N = 81$ ), the measured ground state is reproduced in the shell model calculation as  $4^+$ .

The higher spin negative parity states above the  $8^-$  state in  $^{130,132}\text{I}$ , newly observed in the present work, could be reproduced well in the shell model calculations, as can be seen from Fig. 16(a) and (b), respectively. The spin assignments to the negative parity levels above the  $8^-$  isomeric state in both  $^{130,132}\text{I}$  are based on the comparison with the present shell model calculation and the systematics of the even mass Iodine isotopes. The relative excitation energies and the sequence  $8^- - 10^- - 11^- -$

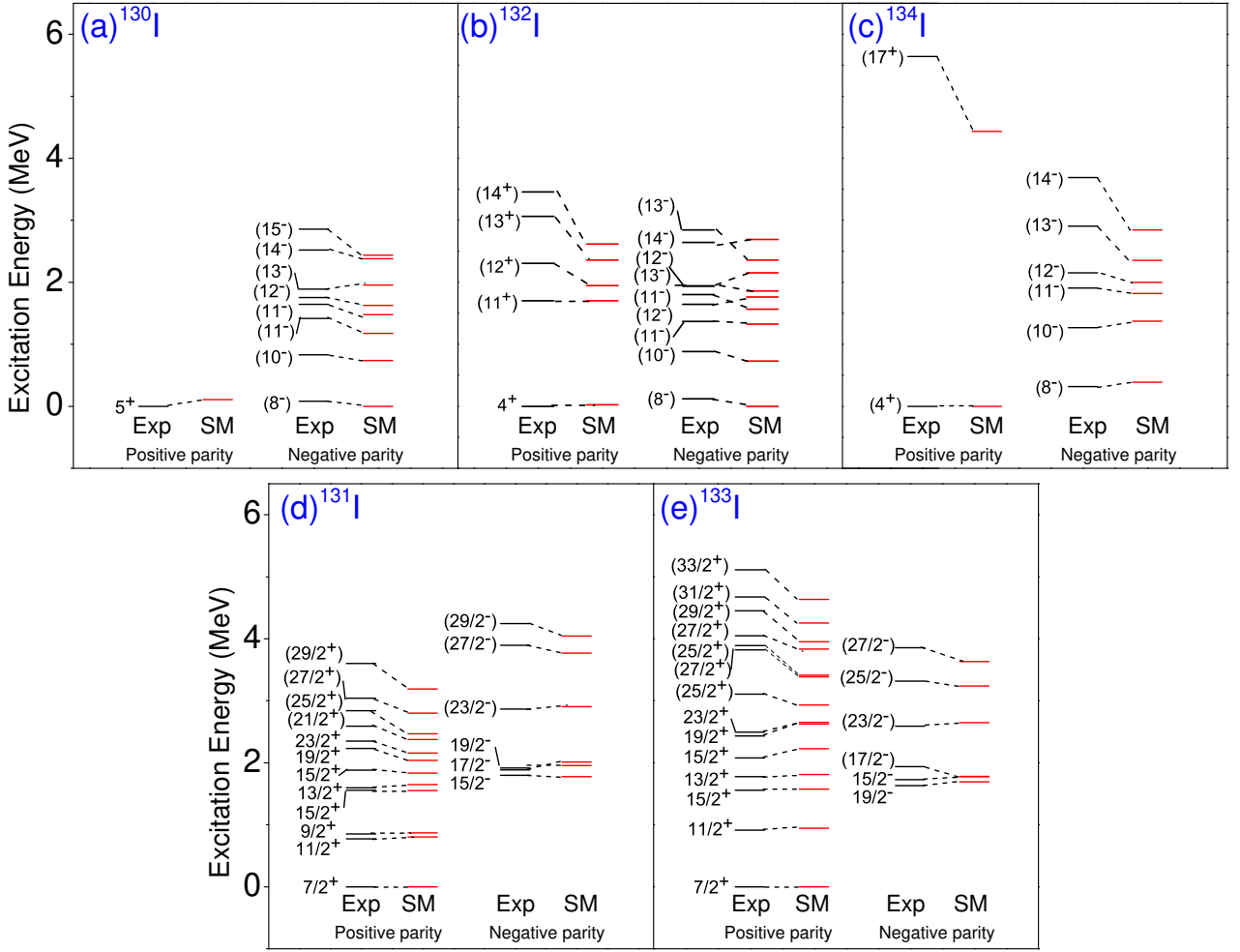


FIG. 16: (Color online) The comparison of experimental ((Exp) shown in black) and theoretical ((SM) shown in red) level schemes for even- $A$   $^{130,132,134}\text{I}$  (a-c) and odd- $A$   $^{131,133}\text{I}$  (d-e) isotopes for both positive and negative parities. The experimental and shell model states of the same spin-parity have been joined with dotted lines to guide the eye.

$12^-$  with respect to the  $8^-$  state in  $^{130,132}\text{I}$  follow a smooth pattern and is very similar to the corresponding states in  $^{128}\text{I}$  ( $N = 75$ ) and  $^{134}\text{I}$  ( $N = 81$ ). Thus the excited states at 830, 1419 and 1752 keV in  $^{130}\text{I}$  and the states at 882, 1367 and 1644 keV in  $^{132}\text{I}$  are assigned as  $10^-$ ,  $11^-$  and  $12^-$  respectively. This relative energy spacing increases for higher mass number towards  $N = 82$ . The yrast sequence  $12^- - 10^- - 8^-$  in  $^{130}\text{I}$  and  $^{132}\text{I}$  also closely follow the analogous sequence of  $15/2^+ - 11/2^+ - 7/2^+$  in odd- $A$  neighbours  $^{129}\text{I}$  and  $^{131}\text{I}$ , respectively.

The new 342 ns isomeric state in  $^{132}\text{I}$ , reported in the present work, is tentatively assigned as  $(11^+)$ , following the systematics of similar isomers observed in even- $A$  Sb isotopes [31]. The three new excited states observed above the  $(11^+)$  isomer in  $^{132}\text{I}$  are assigned as  $(12^+)$ ,  $(13^+)$  and  $(14^+)$ , respectively, following the similar pattern of spin sequence above the  $(11^+)$ , 600 ns isomer, in  $^{130}\text{Sb}$ . The excitation energy of the  $(11^+)$  isomer in  $^{132}\text{I}$  could not be determined experimentally. The shell

model calculation predicts the  $\pi g_{7/2}^3 \nu d_{3/2}^{-1} \nu h_{11/2}^{-2}$  configuration as the main component of those positive parity states with an admixture of  $\pi g_{7/2}^3 \nu s_{1/2}^{-1} \nu h_{11/2}^{-2}$  configuration. The excitation energy differences of the positive parity states, above the  $(11^+)$  isomer are not well reproduced by the shell model calculations (Fig. 16(b)).

In  $^{134}\text{I}$ , the yrast states, *i.e.* ( $8^- - 14^-$ ) were understood as built from the  $\pi g_{7/2}^3 \nu h_{11/2}^{-1}$  and  $\pi g_{7/2}^2 \pi d_{5/2} \nu h_{11/2}^{-1}$  configurations [18, 51]. In this work, the newly observed state at 5644 keV decaying by the emission of the 1955 keV transition, is proposed as  $(17^+)$ , resulting from the  $\pi g_{7/2}^3 \pi h_{11/2}^{-1} \nu h_{11/2}^{-1}$  configuration, based on the following considerations. In the neighboring nucleus  $^{135}\text{I}$ , having the closed  $N = 82$  shell, the low-lying positive parity states, ( $7/2^+$ ,  $11/2^+$ ,  $15/2^+$ ,  $17/2^+$ ), are mainly from the  $\pi g_{7/2}^3$  and  $\pi g_{7/2}^2 \pi d_{5/2}^1$  configurations [19, 52]. The higher-lying yrast states, around 3.7 MeV ( $19/2^-$ ,  $21/2^-$ ,  $23/2^-$ ), have negative parity and are understood as resulting from one proton excitation

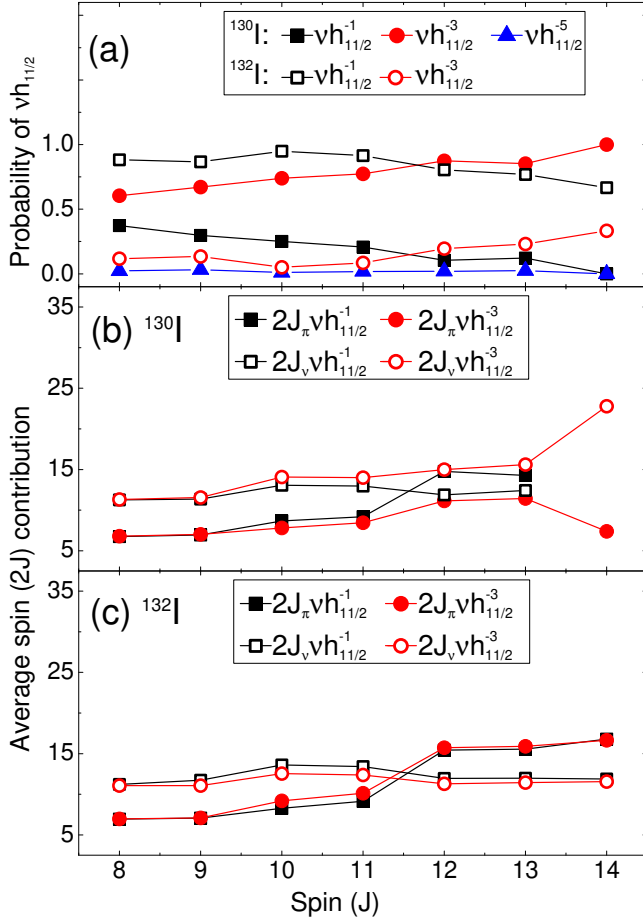


FIG. 17: (a) Probability of neutron hole occupancy in  $\nu h_{11/2}$  orbital for  $^{130,132}\text{I}$  as a function of the total spin ( $J$ ) of the negative parity states, (b) Average spin contribution of proton ( $2J_\pi$ ) and neutron ( $2J_\nu$ ) to the total spin ( $J$ ) of the negative parity states in  $^{130}\text{I}$  for different number of hole occupancy in the  $\nu h_{11/2}$  orbital and (c) Same as (b), but for  $^{132}\text{I}$ .

to the  $\pi h_{11/2}$  orbital, leading to a  $\pi g_{7/2}^2 \pi h_{11/2}$  configuration. The strongest decay of these states to the positive parity states is of  $E3$  nature, corresponding to the  $\pi h_{11/2} \rightarrow \pi d_{5/2}$  stretched  $E3$  transition. An analogous pattern can be also observed in  $^{134}\text{Te}$  [19, 52]. From the results of the shell model calculations, in  $^{135}\text{I}$   $17/2^+$  and  $19/2^-$ ,  $21/2^-$ ,  $23/2^-$  states are (not shown) between 200 and 400 keV lower as compared to the experimental values. In  $^{134}\text{I}$ , the model calculations further under predict the excitation energy of the  $13^-$ ,  $14^-$  and  $17^+$  states (Fig. 16(c)).

For the odd- $A$  Iodine isotopes,  $^{131,133}\text{I}$ , the previously known positive parity states below the  $23/2^+$ ,  $19/2^-$  and  $15/2^-$  isomers have been reproduced well in the present shell model calculations (Fig. 16(d-e)). The excited states above the  $19/2^-$  isomer, in both  $^{131,133}\text{I}$ , are reported for the first time in the present work. The three levels above  $19/2^-$  are assigned as  $(23/2^-)$ ,  $(27/2^-)$  and  $(29/2^-)$  in  $^{131}\text{I}$  and as  $(23/2^-)$ ,  $(25/2^-)$  and  $(27/2^-)$  in

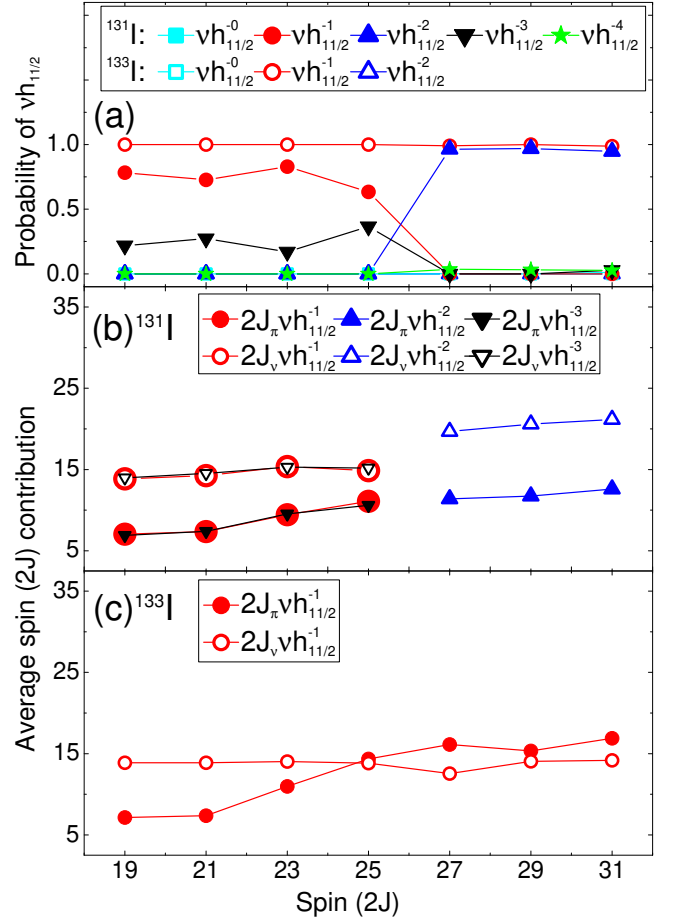


FIG. 18: (a) Probability of neutron hole occupancy in  $\nu h_{11/2}$  orbital for  $^{131,133}\text{I}$  as a function of the total spin ( $2J$ ) of the negative parity states, (b) Average spin contribution of proton ( $2J_\pi$ ) and neutron ( $2J_\nu$ ) to the total spin ( $2J$ ) of the negative parity states in  $^{131}\text{I}$  for different number of hole occupancy in the  $\nu h_{11/2}$  orbital and (c) Same as (b), but for  $^{133}\text{I}$ .

$^{133}\text{I}$ , based on the agreement of the experimental results with the shell model calculation. The level at 1938 keV in  $^{133}\text{I}$  is newly observed in the current work and is connected to  $15/2^+$  level via 378 keV transition. This state is assigned as  $(17/2^-)$ , following a similar assignment of a level, reported earlier in  $^{131}\text{I}$  [17].

We will now focus on the features of the negative parity states,  $(8^- - 14^-)$  in  $^{130,132}\text{I}$  and  $(19/2^- - 31/2^-)$  in  $^{131,133}\text{I}$ . The present shell model calculations show that the proton particles in the  $\pi g_{7/2}$ ,  $\pi d_{5/2}$ ,  $\pi h_{11/2}$  and neutron holes in the  $\nu d_{3/2}$ ,  $\nu s_{1/2}$ ,  $\nu h_{11/2}$  have a leading contribution to the structure of the negative parity excited states. All the other orbitals remain relatively inactive. This work shows that, in case of  $^{130-133}\text{I}$ , the neutron hole occupancy in the  $\nu h_{11/2}$  orbital can undergo variation as a function of the spin of the state, though, as can be seen in  $^{134}\text{I}$  [18, 51], all the states with the relevant spins could be made with only one neutron hole in the  $\nu h_{11/2}$ . In Fig. 17(a) and Fig. 18(a) the probability of

neutron hole occupancy in  $\nu h_{11/2}$  orbital is shown as a function of the total spin ( $J$ ) and ( $2J$ ) of the negative parity states, for  $^{130,132}\text{I}$  and  $^{131,133}\text{I}$ , respectively. It can be seen from the figures that:

- $^{132}\text{I}$  : (three neutron holes) the main contribution is from the  $\nu h_{11/2}^{-1}$ , which slightly decreases at higher spin in favor of the  $\nu h_{11/2}^{-3}$  configuration,
- $^{130}\text{I}$  : (five neutron holes) there is a large contribution of  $\nu h_{11/2}^{-1}$  and  $\nu h_{11/2}^{-3}$  at lower spin, while the  $\nu h_{11/2}^{-3}$  dominates at higher spin, the contribution of  $\nu h_{11/2}^{-5}$  is negligible,
- $^{133}\text{I}$  : (two neutron holes) the  $\nu h_{11/2}^{-1}$  configuration is almost pure,
- $^{131}\text{I}$  : (four neutron holes) the  $\nu h_{11/2}^{-1}$  configuration dominates until  $25/2^-$ , beyond which the  $\nu h_{11/2}^{-2}$  takes over, implying the contribution of the proton  $\pi h_{11/2}$  excitation.

The average spin contribution of proton ( $2J_\pi$ ) and neutron ( $2J_\nu$ ) to the total spin of the negative parity states, for the configurations involving different occupancy of the  $\nu h_{11/2}$  orbital, is shown in Fig. 17(b) for  $^{130}\text{I}$ , (c) for  $^{132}\text{I}$  and in Fig. 18(b) for  $^{131}\text{I}$ , (c) for  $^{133}\text{I}$ . In  $^{132}\text{I}$ , at low spin, the average  $J_\pi^\pi$  is  $7/2^+$  and  $J_\nu^\pi$  is  $11/2^-$ . With the increasing spin  $J$ , the average neutron spin remains almost constant, while the proton spin gradually increases towards the full spin alignment ( $17/2^+$ ) of the three protons in the  $\pi g_{7/2}$  and  $\pi d_{5/2}$  orbitals, *i.e.*  $\left| (\pi g_{7/2}^2; 6^+) \times (\pi d_{5/2}; 5/2^+); 17/2^+ \right\rangle$ . A similar behavior is also observed in  $^{134}\text{I}$  (not shown), where the spin contribution of the single neutron hole in  $\nu h_{11/2}$  is  $11/2^-$ . The average spin contributions for the dominant ( $\nu h_{11/2}^{-1}$ ) configuration and that for the admixture ( $\nu h_{11/2}^{-3}$ ) closely follow each other. In  $^{130}\text{I}$ , the trends are similar for the admixture ( $\nu h_{11/2}^{-1}$ ), which has only a negligible contribution to the  $14^-$  state. For the leading component ( $\nu h_{11/2}^{-3}$ ), the proton spin contribution is smaller, which is compensated by the corresponding increase of the spin of the neutrons. In  $^{133}\text{I}$ , at low spin, the average  $J_\pi^\pi$  is  $7/2^+$  and  $J_\nu^\pi$  is  $7^-$ . The configuration of the  $J_\nu^\pi = 7^-$  corresponds to the  $\nu d_{3/2}^{-1} \nu h_{11/2}^{-1}$ . With the increase of the final spin  $J$ , similarly to the  $^{132}\text{I}$ , the average neutron spin remains almost constant while the proton spin gradually increases towards the full spin alignment. In  $^{131}\text{I}$ , the average spin contribution of protons and neutrons, below  $25/2^-$  is similar to that observed for  $^{133}\text{I}$ . The contributions from the dominant ( $\nu h_{11/2}^{-1}$ ) configuration and the admixture ( $\nu h_{11/2}^{-3}$ ) follow each other. The crossing between the average neutron and proton spin

doesn't occur. At  $27/2^-$ , the configuration changes to  $\nu h_{11/2}^{-2}$  and one proton is promoted to the  $\pi h_{11/2}$  orbital. The average spin of protons  $J_\pi^\pi$  is  $11/2^-$  and that of neutrons  $J_\nu^\pi$  is  $10^+$ . The predicted, sudden change of the configuration, involving the  $\pi h_{11/2}$  excitation could however occur at too low excitation energy in the model, as already discussed earlier for  $^{134}\text{I}$ . These shell model calculations, for the negative parity states of  $^{130-134}\text{I}$  in terms of their neutron and proton occupancies and spins were discussed. The importance of the hole occupancy of  $\nu h_{11/2}$  orbital in generation of the high spin negative parity states in these I isotopes was shown.

## V. SUMMARY

The prompt-delayed spectroscopy of neutron-rich Iodine isotopes  $^{130-134}\text{I}$  was carried out after producing the nuclei in fusion-fission and transfer induced fission of the reaction  $^9\text{Be} (^{238}\text{U}, f)$  at a beam energy of 6.2 MeV/u. The prompt transitions above the isomers in odd-odd  $^{130,132}\text{I}$  have been identified for the first time and a new isomer in  $^{132}\text{I}$  is reported. The level scheme of  $^{134}\text{I}$  is also extended. The high spin level structure of  $^{131,133}\text{I}$  have been extended with the placement of new prompt transitions above the known isomers. The proposed level schemes are interpreted in terms of systematics and large scale shell model calculations. It is found that, the hole occupancy in the  $\nu h_{11/2}$  orbital plays a dominant role in generating the high spin negative parity states in these neutron rich Iodine isotopes. An additional feature, that the hole occupation of the  $\nu h_{11/2}$  orbital vary strongly in certain I isotopes could also be observed.

## VI. ACKNOWLEDGMENTS

The authors gratefully acknowledge the AGATA collaboration for the availability of the AGATA  $\gamma$  tracking array at GANIL. We would like to thank the GANIL accelerator staff for their technical contributions. We thank A. O. Macchiavelli for help in data collection during the experiment. SB, SB and RB acknowledge the support received from CEFIPRA project No. 5604-4 and SB, RP acknowledge the support from LIA France-India agreement. PB and AM acknowledge support from the Polish National Science Centre (NCN) under Contract No. 2016/22/M/ST2/00269 and the French LEA COPI-GAL project. HLC and PF acknowledge support from the U.S. Department of Energy, Office of Science, Office of Nuclear Physics under Contract No. DE-AC02-05CH11231 (LBNL). RMPV acknowledge partial support by Ministry of Science, Spain, under the grants BES-2012-061407, SEV-2014-0398, FPA2017-84756-C4 and by EU FEDER funds.

- 
- [1] J. P. Schiffer and W. W. True, *Rev. Mod. Phys.* **48**, 191 (1976).
- [2] L. Coraggio, et al., *Phys. Rev. C* **66**, 64311 (2002).
- [3] L. Coraggio, et al., *Nucl. Phys. A* **805**, 424 (2008).
- [4] B. Fogelberg, et al., *Phys. Rev. Lett.* **73**, 2413 (1994).
- [5] K. L. Jones, et al., *Nature* **465**, 454 (2010).
- [6] M. Rejmund, et al., *Phys. Lett. B* **753**, 86 (2016).
- [7] S. Biswas, et al., *Phys. Rev. C* **93**, 34324 (2016).
- [8] J. Genevey, et al., *Phys. Rev. C* **65**, 034322 (2002).
- [9] P. Bhattacharyya, et al., *Phys. Rev. Lett.* **87**, 62502 (2001).
- [10] L. Coraggio, et al., *Phys. Rev. C* **87**, 34309 (2013).
- [11] H. Kaur, et al., *Phys. Rev. C* **55**, 512 (1997).
- [12] H. Kaur, et al., *Phys. Rev. C* **55**, 2234 (1997).
- [13] B. Kanagalekar, et al., *Phys. Rev. C* **88**, 54306 (2013).
- [14] B. Ding, et al., *Phys. Rev. C* **86**, 34302 (2012).
- [15] B. Ding, et al., *Phys. Rev. C* **85**, 44306 (2012).
- [16] D. Deleanu, et al., *Phys. Rev. C* **87**, 14329 (2013).
- [17] H. Watanabe, et al., *Phys. Rev. C* **79**, 64311 (2009).
- [18] S. H. Liu, et al., *Phys. Rev. C* **79**, 67303 (2009).
- [19] S. K. Saha, et al., *Phys. Rev. C* **65**, 017302 (2001).
- [20] W. Urban, et al., *Eur. Phys. J. A* **27**, 257 (2006).
- [21] T. Rząca-Urban, et al., *Phys. Rev. C* **75**, 054319 (2007).
- [22] A. Korgul, et al., *Eur. Phys. J. A* **12**, 129 (2001).
- [23] W. Urban, et al., *Phys. Rev. C* **65**, 024307 (2002).
- [24] A. Navin, et al., *Phys. Lett. B* **728**, 136 (2014).
- [25] M. Rejmund, et al., *Nucl. Instr. Meth. Phys. Res. A* **646**, 184 (2011).
- [26] A. Navin and M. Rejmund, in *McGRAW-HILL Yearb. Sci. Technol.* (2014) p. 137.
- [27] M. Vandebrouck, et al., *Nucl. Instr. Meth. Phys. Res. A* **812**, 112 (2016).
- [28] Y. H. Kim, et al., *Eur. Phys. J. A* **53**, 162 (2017).
- [29] S. Akkoyun, et al., *Nucl. Instr. Meth. Phys. Res. A* **668**, 26 (2012).
- [30] J. Simpson, et al., *Acta Physica Hungarica New Series Heavy Ion Physics* **11**, 159 (2000).
- [31] S. Biswas, et al., *Phys. Rev. C* **99**, 64302 (2019).
- [32] S. L. Sakharov, et al., *Nucl. Phys. A* **494**, 36 (1989).
- [33] P. Puppe, et al., *Phys. Rev. C* **86**, 44603 (2012).
- [34] B. Singh, *Nucl. Data Sheets* **93**, 33 (2001).
- [35] S. V. Jackson, et al., *Phys. Rev. C* **11**, 1323 (1975).
- [36] G. Lhersonneau, et al., *Phys. Rev. C* **12**, 609 (1975).
- [37] E. S. Macias and W. B. Walters, *Nucl. Phys. A* **161**, 471 (1971).
- [38] R. L. Auble, et al., *Phys. Rev.* **169**, 955 (1968).
- [39] M. Dikić, et al., *Phys. Rev. C* **10**, 1172 (1974).
- [40] S. K. Das, et al., *Eur. Phys. J. A* **4**, 1 (1999).
- [41] S. Bhattacharyya, et al., *EPJ Web of Conferences* **66**, 02009 (2014).
- [42] M. Tanigaki, et al., *Phys. Rev. C* **80**, 34304 (2009).
- [43] H. G. Hicks, et al., *Phys. Rev. C* **27**, 2203 (1983).
- [44] W. B. Walters, et al., *Phys. Rev. C* **29**, 991 (1984).
- [45] R. A. Meyer, et al., *Phys. Rev. C* **13**, 1617 (1976).
- [46] V. Berg and A. Höglund, *Nucl. Phys. A* **175**, 495 (1971).
- [47] A. A. Sonzogni, *Nuclear Data Sheets* **103**, 1 (2004).
- [48] C. D. Coryell, et al., *Nucl. Phys. A* **179**, 689 (1972).
- [49] B. Brown and W. Rae, *Nucl. Data Sheets* **120**, 115 (2014).
- [50] B. A. Brown, et al., *Phys. Rev. C* **71**, 44317 (2005).
- [51] L. Coraggio, et al., *Phys. Rev. C* **80**, 061303 (2009).
- [52] C. T. Zhang, et al., *Phys. Rev. Lett.* **77**, 3743 (1996).